# Interface nano-optics with van der Waals polaritons

https://doi.org/10.1038/s41586-021-03581-5

Received: 7 June 2020

Accepted: 23 April 2021

Published online: 8 September 2021

Check for updates

Qing Zhang[1,7], Guangwei Hu[1,7], Weiliang Ma[2], Peining Li[2], Alex Krasnok[3], Rainer Hillenbrand[4,5], Andrea Alù[3,6]✉ & Cheng-Wei Qiu[1]✉

Polaritons are hybrid excitations of matter and photons. In recent years, polaritons in van der Waals nanomaterials—known as van der Waals polaritons—have shown great promise to guide the flow of light at the nanoscale over spectral regions ranging from the visible to the terahertz. A vibrant research field based on manipulating strong light–matter interactions in the form of polaritons, supported by these atomically thin van der Waals nanomaterials, is emerging for advanced nanophotonic and opto-electronic applications. Here we provide an overview of the state of the art of exploiting interface optics—such as refractive optics, meta-optics and moiré engineering—for the control of van der Waals polaritons. This enhanced control over van der Waals polaritons at the nanoscale has not only unveiled many new phenomena, but has also inspired valuable applications—including new avenues for nano-imaging, sensing, on-chip optical circuitry, and potentially many others in the years to come.

Controlling light at the nanoscale has long been a pursuit of the nanophotonics community. The recent emergence of layered van der Waals (vdW) materials has opened new avenues for the extreme control of light down to the atomic length-scale, because such materials support quasi-particle half-light and half-matter excitations—known as polaritons—that exhibit long lifetimes, low loss and strong field confinement[1–3]. Polaritons in vdW materials with enhanced light–matter interactions facilitate promising nanophotonic applications, such as sensing[4–6], nanoimaging[7–9], optical modulation[10–14], light emission and lasing[15–17].

Research into polaritons in natural vdW materials includes the study of monolayers, thin slabs and hybrid heterostructures[18–23], paving the way to a plethora of new photonic device concepts and applications, as described in previous review articles[1–3]. To fully develop the potential of vdW polaritons, it is important to understand and tailor their propagation over interfaces. Such propagation is determined by their dispersion features characterized by iso-frequency contours (IFCs) in reciprocal space (Box 1 and Fig. 1a). In this Review, we focus exclusively on the extreme manipulation of polaritons in artificially engineered vdW materials and their hybrid systems over an interface—including individual cavities, waveguides, photonic crystals, metasurfaces and, recently, moiré bilayers. All of these techniques establish the basis for a new research area of interface optics, which can be divided into three approaches of polariton control (Fig. 1c–e), namely refractive optics, meta-optics and moiré engineering. In the following sections, we first review the available techniques used to detect and image vdW polaritons (Box 2). Next we discuss recent progress in the control of polariton propagation via refractive optics (Fig. 1c), and highlight functionalities that are implemented using this approach, such as polariton lenses, prisms and negative refraction. Then we describe state-of-the-art meta-optics (Fig. 1d) and nanostructuring of vdW polaritons for arbitrary wavefront control, resonant cavity and dispersion engineering. Finally, we review emerging techniques of moiré engineering and interlayer effects in vdW bilayers (Fig. 1e), which provide alternative control mechanisms in polaritonic response with unique nanophotonic and quantum phenomena, including photonic crystal nanolight, polariton canalization and topological transitions. Last, we discuss developing trends and practical applications of this emerging research area and offer our projections for the future.

## Refractive optics

In free space, refractive optics relies on bulk transparent diffractive optical elements to achieve phase control. For instance, conventional focusing lenses require curved shapes to achieve optical path difference and hence phase accumulation. Polaritons sustained in vdW materials are near-field phenomena, however, and can be manipulated with inspiration from free-space technologies. By mimicking conventional refractive optics, it is possible to realize the steering and focusing of polaritons[29,45]. This is possible because polaritons in vdW materials are highly tunable, and their optical path differences can be modified in terms of their propagation constant ($n_{\mathrm{eff}}k_0$) and propagation trajectory. Polaritons are strongly sensitive to the dielectric environment, which can therefore be manipulated via reconfiguring the substrate with, for example, phase-change materials such as $VO_2$ (Fig. 2a). In addition, polaritons in graphene can be modified by electrical doping[46] (red lines in Fig. 2b). In this way, the focusing of phonon polaritons in hexagonal boron nitride (hBN) slabs was first numerically predicted by a curved boundary at the interface of hBN and $VO_2$ with different crystalline phases[45] (Fig. 2c, d), and was later experimentally demonstrated with

[1]Department of Electrical and Computer Engineering, National University of Singapore, Singapore, Singapore. [2]Wuhan National Laboratory for Optoelectronics and School of Optical and Electronic Information, Huazhong University of Science and Technology, Wuhan, China. [3]Advanced Science Research Center, City University of New York, New York, NY, USA. [4]CIC nanoGUNE BRTA and Department of Electricity and Electronics, UPV/EHU, Donostia-San Sebastián, Spain. [5]IKERBASQUE, Basque Foundation for Science, Bilbao, Spain. [6]Physics Program, Graduate Center, City University of New York, New York, NY, USA. [7]These authors contributed equally: Qing Zhang, Guangwei Hu. ✉e-mail: aalu@gc.cuny.edu; chengwei.qiu@nus.edu.sg

## Box 1

# In-plane dispersion of natural van der Waals polaritons

Assuming that the involved vdW materials are non-magnetic and feature a linear response in the intensity regime of interest, the iso-frequency contours (IFCs) can be modelled by the anisotropic permittivity tensor $\hat{\varepsilon} = \mathrm{diag}\,[\varepsilon_x, \varepsilon_y, \varepsilon_z]$, in which $\varepsilon_x$, $\varepsilon_y$ are the in-plane components within the interface and $\varepsilon_z$ is the out-of-plane component perpendicular to the interface (Fig. 1a). A circular (closed) IFC for the emerging polaritons propagating on the surface can be found in uniaxial materials with in-plane isotropy ($\varepsilon_x = \varepsilon_y \neq \varepsilon_z$), such as plasmon polaritons in monolayer graphene ($\varepsilon_x = \varepsilon_y < 0$)[27,28,122] (Fig. 1b, left), phonon polaritons in hexagonal boron nitride (hBN) ($\varepsilon_x = \varepsilon_y$, $\varepsilon_x\varepsilon_z < 0$)[8,30,123,125], exciton-polaritons in transition metal dichalcogenides ($\varepsilon_x = \varepsilon_y \neq \varepsilon_z > 0$)[126]. More exotic features emerge when considering in-plane anisotropic vdW materials ($\varepsilon_x \neq \varepsilon_y$), including elliptical plasmons in semiconductor black phosphorus ($\varepsilon_x \neq \varepsilon_y < 0$)[119,127] and highly directional ray-like hyperbolic plasmons in black phosphorus[128] and $WTe_2$ thin films ($\varepsilon_x\varepsilon_y < 0$)[129]. In addition, in-plane hyperbolic and elliptical phonon polaritons have been observed in the natural biaxial vdW material α-$MoO_3$[35,88,130,131] (Fig. 1b, right) and in α-$V_2O_5$[132]. Near the transition from hyperbolic to elliptical dispersion, the IFCs flatten, leading to highly collimated diffractionless canalized modes[55–57,84,86,87], corresponding to propagation along one specific direction due to the constant group velocity $\vec{v_g} = \nabla\omega(\vec{k})$. Polariton IFCs with circular, elliptical and hyperbolic topologies can be achieved with general dispersion[133,134], $q = \frac{\rho}{k_0 d}\left[\arctan\left(\frac{\varepsilon_1\rho}{\varepsilon_z}\right) + \arctan\left(\frac{\varepsilon_3\rho}{\varepsilon_z}\right) + \pi l\right]$, $l = 0,\ 1,\ 2\ldots$, in which $\rho = i\sqrt{\varepsilon_z q^2/(\varepsilon_x q_x^2 + \varepsilon_y q_y^2)}$, $m$ denotes the modal order, $q^2 = (k_x/k_0)^2 + (k_y/k_0)^2$ is the normalized in-plane momentum, $d$ is the vdW slab thickness, and $\varepsilon_1$, $\varepsilon_3$ are the permittivities of the superstrate and substrate, respectively. When considering twisted vdW bilayers, the dispersion relation is more complex and can be analytically calculated by considering the coupling of the two layers separated by a spacer[56,84,86,87].

another phase-change material $Ge_3Sb_2Te_6$ (GST)[34]. Another typical example is the graphene plasmon refraction based on spatial conductivity patterns[47] (Fig. 2e). By changing the carrier density within the prism (pink) domain, the propagating graphene plasmon undergoes positive refraction at the prism boundary due to the different effective mode index $n_{\mathrm{eff}}$ of graphene plasmon modes in and outside the prism. In one experiment[29], a graphene bilayer was used to act as a prism, and the wavefront was tilted by 24° outside the left prism boundary (Fig. 2f). In-plane all-angle negative refraction in lateral heterojunctions of hBN and graphene has also been numerically studied[48] (Fig. 2g). Owing to its natural hyperbolicity, hBN supports type-I phonon polaritons featuring negative phase velocity (with deceasing dispersion slope in Fig. 2b) within its first reststrahlen band[30]. When such phonon polaritons travel to the monolayer graphene, the refracted graphene plasmon remains on the same side of the normal, resulting in negative refraction (Fig. 2h). This phenomenon of negative refraction has also inspired a new way for developing momentum-matching diffractive optical elements. One example is a flat Luneburg lens in a curved heterojunction with graphene and hBN[49]. The same magnitude of $n_{\mathrm{eff}}$ between positive and negative index polaritons ensures momentum matching, but the opposite signs of $n_{\mathrm{eff}}$ results in a gradual phase accumulation that leads to polariton focusing.

### Meta-optics

Unlike refractive optics, which uses the optical path difference in bulk elements to achieve phase control, meta-optics has emerged as a versatile method for engineering polariton propagation by nanopatterning either the environment or the vdW layers. For instance, individual VdW nanocavities (for example nanoribbons, nanorods, nanodiscs) have demonstrated great potential for tailoring propagating and localized polariton modes[7,31,50] (Fig. 3a–c), especially in the case of edge-oriented and steerable phonon polaritons in anisotropic α-$MoO_3$ nanocavities[51]. These nanocavities can be used for nanophotonic and thermal applications, such as surface-enhanced infrared molecular absorption[4,6], deeply subwavelength light waveguiding[52] and ultrafast heat transfer[53,54]. When the distance between adjacent vdW nanostructures is smaller than the decay length of polaritons, an array of vdW nanostructures can be collectively coupled, forming a metasurface that can be used to manipulate artificial polariton modes. A representative metasurface structure is an array of vdW nanoribbons (for example, graphene or hBN nanoribbons)[32,55,56] (Fig. 3d). Such a metasurface exhibits strong in-plane anisotropy and hence supports polaritons with two different types of anisotropic in-plane dispersion: elliptical dispersion ($\varepsilon_{\mathrm{eff},x} \neq \varepsilon_{\mathrm{eff},y} < 0$) and hyperbolic dispersion ($\varepsilon_{\mathrm{eff},x}\varepsilon_{\mathrm{eff},y} < 0$). A hallmark feature of in-plane hyperbolic polaritons is their anomalous concave wavefront, which can be visualized by near-field polariton imaging[36] (Fig. 3e). By sweeping the frequency, a topological transition from hyperbolic to elliptical dispersion can be obtained in the metasurface, as $\varepsilon_{\mathrm{eff},x}$ or $\varepsilon_{\mathrm{eff},y}$ change sign. This yields various intriguing phenomena, such as the marked enhancement of photonic local density of states and canalization that leads to hyperlensing[55]. The underlying physics behind the topological transition can be explained by the formation of a synthetic transverse optical phonon resonance induced by strong polaritonic coupling between neighbouring nanoribbons[57]. Near the synthetic transverse optical frequency (transition point), the metasurface supports canalized polaritons with diffractionless propagation (Fig. 3f, g), offering opportunities for sub-diffraction imaging, near-field energy transport and super-Coulombic atom–atom interactions[58].

Beyond one-dimensional gratings of vdW nanostructures, vdW polaritonic photonic crystals[59,60]—which exhibit polaritonic bandgaps—can provide new opportunities for manipulating light–matter interactions at the subwavelength scale. Owing to the inherently thin nature of these materials, the polariton fields are spread in the surrounding dielectric environment. By periodic structuring of the dielectric substrate, polaritonic crystals can be structured without the need of etching and thus potentially avoiding damaging the vdW materials (Fig. 3h). As a result, one-dimensional propagation of graphene plasmons has been experimentally demonstrated in such dielectric-loaded graphene photonic crystals, which can be further modulated by tuning the gate voltage[60] (Fig. 3i). Furthermore, by using phase-change materials (for example, GST) as switchable meta-atoms to achieve tunable phase control (Fig. 3j), it may also be possible to realize reconfigurable planar metalens to manipulate polaritons[34] (Fig. 3k). In experiments, a subwavelength laser spot was used to write and erase patterns on the GST films with high spatial resolution. The different phase domains of GST can be written and rewritten many times[61]. In this way, the GST metasurface is dynamic and in-situ tunable, which paves the way towards reconfigurable and programmable meta-devices for vdW polaritons.

### Interlayer effects and moiré engineering

After a single vdW crystal is realized, its intrinsic electronic band structures and optoelectronic properties are solely controlled by its atomic structure, assuming the absence of strain or external magnetic bias. Stacking two layers, however, establishes new atomic arrangements, which can lead to interesting properties resulting from the interlayer effect and as a result of moiré engineering. Moiré patterns are formed

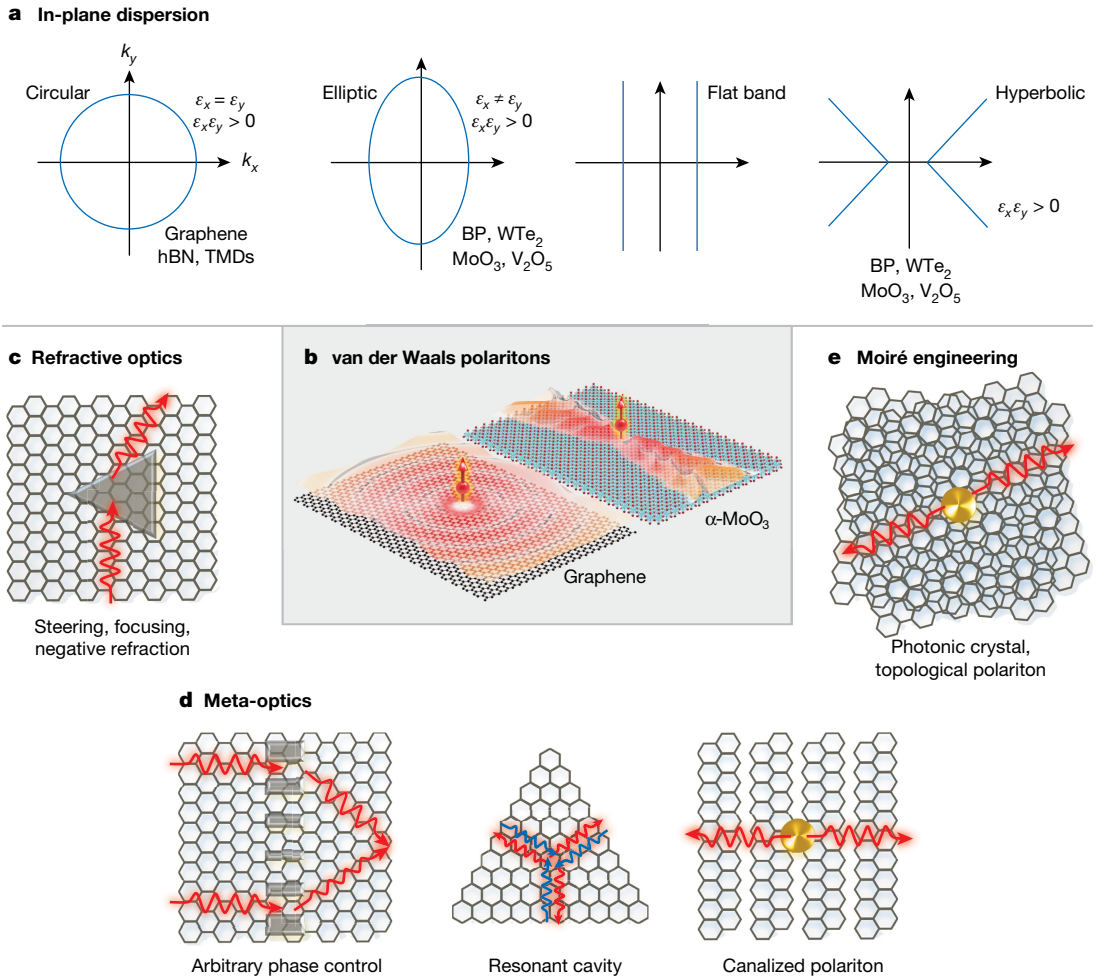


**Fig. 1 | Interface optics with vdW polaritons. a**, In-plane dispersion of various types of vdW polariton. **b**, Schematic of propagating surface plasmon polaritons over graphene (isotropic), and hyperbolic phonon polaritons over α-$MoO_3$ (hyperbolic). **c**, Planar refractive optics enables functions such as polariton prisms, lenses and negative refraction. **d**, Meta-optics for vdW polaritons. Metasurfaces composed of phase-change material nanostructures coupled to vdW layers offer phase control of propagating polaritons (left); nanostructuring of vdW materials enables individual resonant cavities (middle) and opens up the opportunity of dispersion engineering (right) for topological transitions and canalized polaritons. **e**, Moiré engineering realizes photonic crystal nanolight and topological polaritons in twisted vdW bilayers.

by lattice misalignment or mismatch between adjacent atomic layers, such as in twisted bilayers[62–67] or lattice mismatch bilayers (for example, graphene/hBN[32]). Such patterns result in long-range interlayer coupling that substantially modifies the electronic structure and material properties. In electronics, the outcome of such interlayer hopping includes the possibility of inducing a flat band structure that supports superconductivity, as demonstrated in twisted bilayer graphene (TBG)[62,63], and moiré excitons due to band structure hybridization in twisted bilayer transition metal dichalcogenides[64–67]. These discoveries at atomic electronic interfaces have sparked curiosity and inspired the investigation of photonic and polaritonic band structure engineering with interlayer coupling in vdW interfaces.

One important interlayer effect for photonics is strain, both triggered and spontaneously arising between two stacked layers. For example, two distinct orderings of degenerate lowest-energy stacking of atomic lattices—that is, AB and BA stacking—exist in bilayer graphene[68]. When any shift or misalignment occurs between the bilayers, a soliton-like domain wall with strain is introduced near the transition of two coexisting but spatially separated lowest-energy stacking orders, as shown in Fig. 4a. Besides the discovery in electronics of topologically protected quantum valley Hall edge states[69,70], it has also been found that graphene plasmons are strongly reflected at these domain walls[71,72] (Fig. 4b). Therefore, in TBGs with small rotation angles, a moiré superlattice with a periodicity close to the graphene plasmon wavelength is formed, introducing a series of graphene plasmon reflections in periodic soliton domain walls—essentially a photonic crystal for graphene plasmons[33]. Such photonic crystal plasmons can be visualized by using s-SNOM, as shown schematically in Fig. 4c. The experimentally measured near-field pattern varies periodically at the moiré domain walls, which gives a real-space reconstruction of the electronic structure of the superlattice (Fig. 4d). Beyond s-SNOM based nano-imaging[73–76], nanophotocurrent mapping[77] and piezoresponse force microscopy[78] have also been applied to characterize the local structure of moiré superlattices. More recently, many new plasmonic effects have been predicted to emerge from interlayer quantum coupling in TBGs, such as intrinsically undamped plasmons in narrow-band electronic systems of TBG[79] and two-dimensional electron gas[80]. Such undamped plasmons are, in principle, immune to Landau damping; this is central for the ongoing quest for low-loss plasmons. Besides, the plasmonic Dirac cone[81] has also been theoretically investigated in TBGs, offering a means through which to manipulate graphene plasmons. These interlayer effects on plasmons can be scaled up to multilayer systems[71] and potentially extended to polar dielectric vdW crystals for dispersion manipulation of phonon polaritons[74] and hybrid systems[32,75,82]; this will require both theoretical and experimental efforts in the future. In addition, a large set of quantum many-body Hamiltonians can be engineered and controlled

## Box 2

# Detection and visualization of vdW polaritons

**Far-field spectroscopy**

This technique can be applied to study vdW polaritons by patterning either the vdW layers or their environment in form of periodic or isolated nanostructures[24–26], which compensate the large momentum mismatch between free-space photons and polaritons and hence enable efficient coupling between them. The polariton features can be probed by far-field spectroscopy of the transmitted, reflected or scattered light, using standard techniques such as Fourier transform infrared spectroscopy, terahertz time-domain and grating-based spectroscopy.

**Near-field microscopy**

This approach enables imaging the propagation of vdW polaritons in real space, typically achieved with scattering-type scanning near-field optical microscopy (s-SNOM), in which the atomic force microscope tip is illuminated by light and the tip-scattered light is recorded as a function of tip position. With s-SNOM, polaritons can be visualized in two ways: first, polaritons are launched by the s-SNOM tip, which concentrates the illuminating field to a nanoscale spot at its apex, thus providing the necessary momentum. The polaritons are reflected back to the tip at discontinuities (for example, edges, domain walls, defects, holes) and interfere at the tip apex with the local field. Recording the tip-scattered field yields interference fringes with spacing $\lambda_p/2$ (refs. [27,28]), in which $\lambda_p$ is the polariton wavelength. Alternatively, polaritons can be directly launched by an antenna[29] or by the sample edges[30], which then propagate along the interface and scatter at the tip. Recording the tip-scattered field yield images exhibiting polariton interference fringes of spacing $\lambda_p$. Thus far, the main application of 'tip-launched' polariton interferometry has been the imaging of polaritons on unstructured layers[27,28], individual cavities[7,31] and moiré patterns[32,33], whereas 'antenna-launched' wavefront mapping has been used to observe polariton refraction[29], focusing[29,34], and in-plane hyperbolic modes[35,36]. The studies that we discuss on polariton mapping on structured vdW layers are mostly based on s-SNOM. Near-field photocurrent nanoscopy[37–39] is another technique for the imaging ofpolaritons via measuring the photocurrent and can show propagation, thermal diffusion and thermoelectric generation of polaritons. In addition, photothermal infrared microscopy[40] and photoinduced force infrared microscopy[41] are related techniques to image polaritons, in which polariton-induced local heating or optical-forces are recorded via the mechanical response of the atomic force microscope cantilever.

**Electron energy-loss spectroscopy in scanning transmission electron microscopy**

Electron energy-loss spectroscopy in scanning transmission electron microscopy has also been used to investigate phonon polaritons in hBN[42,43] and in an α-$MoO_3$ slab[44]. Through detecting the energy loss of low-angle-scattered electrons, properties of excited polaritons can be extracted. Electron energy-loss spectroscopy can extend the frequency of interest to the far-infrared region, in which continuous-wave laser sources with properties adequate for s-SNOM measurements are lacking. Similar to s-SNOM, the electron beam excites polaritons, which reflect at discontinuities. Recording energy loss as a function of electron beam position yields polariton interference fringes with a spacing of $\lambda_p/2$. This technique, however, cannot perform wavefront mapping, as is possible using s-SNOM.

using moiré heterostructures, providing a robust quantum simulation platform that enables the study of strongly correlated physics and topology in quantum materials[83].

Another possibility is to establish an electromagnetic interlayer coupling for extreme dispersion engineering of polaritons at vdW interfaces. Such a system is closely connected to our previous discussion on meta-optics, as it can induce extreme anisotropy and manipulate the polaritonic dispersion via structuring, as demonstrated in nanostructured graphene[55] and hBN interfaces[36,57] (Fig. 3f). Further, through the twisted stacking of these hyperbolic polaritonic bilayers, the interlayer coupling of evanescent waves is different along different directions due to the in-plane anisotropy, thus making dispersion engineering possible. This was theoretically predicted in twisted bilayers of deeply subwavelength graphene nanoribbons (Fig. 4e), enabling rich and controllable dispersion through variation of the rotation angle[84,85]. The in-plane hyperbolic-to-elliptic topological transition is achieved via the rotation (Fig. 4f), characterized by the integer number of anti-crossing points ($N_{ACP}$) at which the two dispersion lines of the individual layers cross in momentum space. When this number is two the dispersion is hyperbolic, and when it is four the dispersion is elliptic. At the critical twist angle at which $N_{ACP}$ changes, a topological transition arises in the coupled mode dispersion and the evanescently coupled polaritons necessarily become flattened, supporting highly collimated and diffractionless canalized polaritons. This critical twist angle is known as the 'photonic magic angle', in analogy to the magic angle at which a flat Fermi surface is achieved in TBG. This theoretical prediction was later experimentally demonstrated by the same group[56] and was further confirmed by others[86,87] using twisted bilayered α-$MoO_3$ (Fig. 4g), a van der Waals nanomaterial that is naturally endowed with in-plane hyperbolic phonon polaritons[35,88]. A hyperbolic-to-elliptical topological transition can be observed using real-space nanoimaging techniques as the rotation angle is changed at a fixed frequency, along with the canalized flat-band polaritons near photonic magic angles. Over a broad range of frequencies, the magic angle assumes different values. In general, the evanescent interlayer coupling enables extreme dispersion engineering of interface vdW polaritons, which may be extended to many other material platforms for various applications.

## Practical applications and future perspectives

The study of interface optics in vdW polariton systems is still in its early stages but offers a very promising future. Interface optics phenomena based on vdW polaritons can lead to as yet unexplored opportunities for nanophotonics, optoelectronics and topological optics with applications in nano-imaging, biosensors and integrated optical circuits. We envision that such research will encourage new ideas and directions in this emerging area, such as transformation optics and electron–polariton interactions, which may contribute to many emerging applications and offer valuable new technologies. Below we discuss some of these potential applications and offer an outlook to future trends.

## Transformation and topological polaritonics

Currently, reconfigurable polariton metalenses have been realized through direct laser-writing of phase-change materials on the topside of hBN[34] (Fig. 3k). One opportunity is to introduce such spatial dispersion engineering to implement transformation optics for vdW polaritons[47]. In free space, the combination of transformation optics[89] with metamaterials and metasurfaces provides a powerful platform to realize many optical functions that are not available in nature, and one well-known example is invisibility cloaks that can render an object undetectable to outside observers[90,91]. Here, transformation optics for in-plane polaritons may enable us to obtain the distribution of effective index in space to realize specific polariton fields of choice (Fig. 5a). As such, the spatial local refractive index of a polariton cloaking device

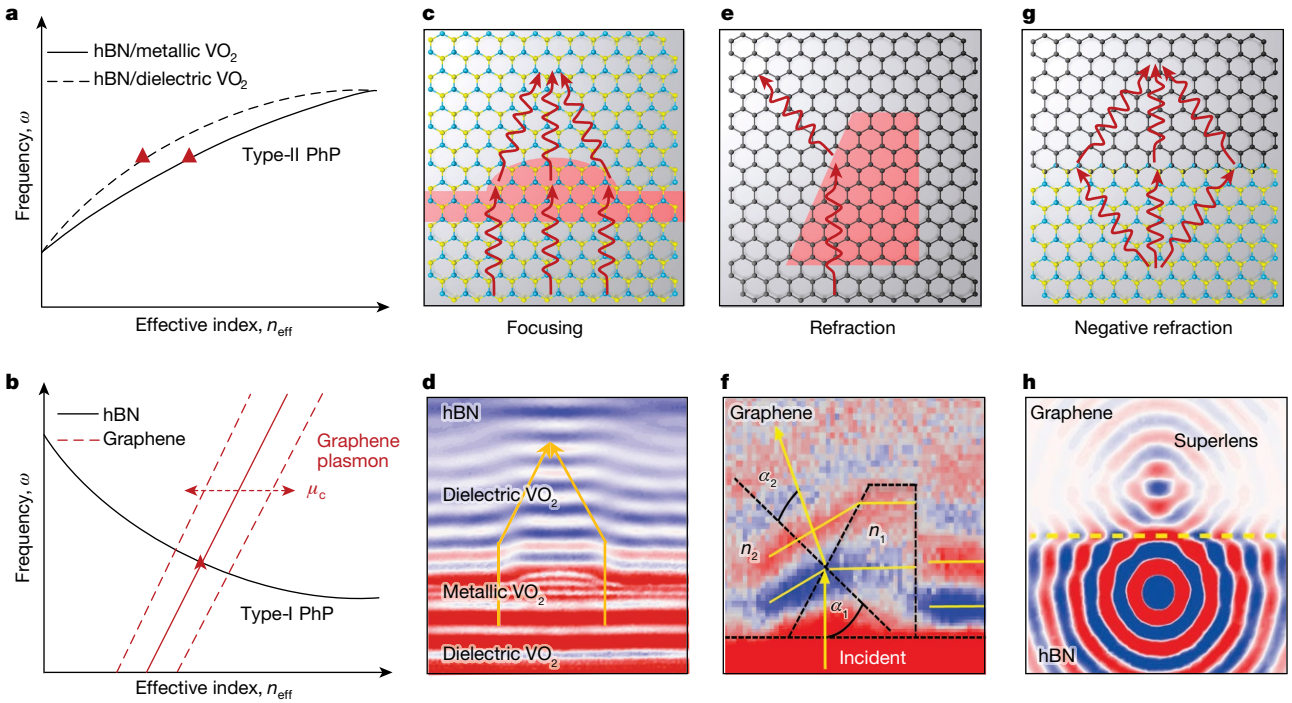


**Fig. 2 | Refractive optics based on planar polaritonic elements.** **a**, Dispersion of hBN type-II phonon polaritons (PhPs) on different $VO_2$ substrates, metallic phase (solid black line) and dielectric phase (dashed black line). **b**, Dispersion of hBN type-I phonon polaritons (black line) with a negative phase velocity, and the dispersion of graphene plasmons (red lines) are electrically tuned by controlling the Fermi level ($\mu_c$) of graphene. **c**, **d**, Reconfigurable polariton focusing by engineering a semi-circular lens of metallic $VO_2$. **e**, **f**, Graphene plasmon refraction based on spatial conductivity patterns. Owing to the contrast in $n_{eff}$ between the background (grey) and the prism (pink) domains, the propagating graphene plasmon undergoes positive refraction at the prism boundary. **g**, **h**, Polaritonic all-angle negative refraction in a lateral heterojunction of hBN and graphene. **d**, Image (simulation) adapted from ref. [45], Springer Nature. **f**, Image (experiment) adapted from ref. [29], AAAS. **h**, Image (simulation) adapted from ref. [48], Lin, X. et al. *Proc. Natl Acad. Sci. USA* **114**, 6717–6721 (2017).

may be achieved through programmable gate arrays on graphene[46,47] or laser-writing of phase-change material patterns on hBN[34]. In addition, an electrostatically tunable plasmon bandgap has been experimentally demonstrated in dielectric-load graphene photonic crystals[60] (Fig. 3i). Another recent research focus has involved extending the concept of nanostructuring of vdW metasurfaces for topological polaritonics (Fig. 5b). This may enable topologically robust and unidirectional edge polariton transport at the interface between two polaritonic crystal domains characterized by distinct topological invariants. Currently, topologically protected plasmons have been predicted in nanostructured graphene layers[92], and helical topological exciton-polaritons have been demonstrated by coupling monolayer TMDs to a nontrivial photonic crystal[93]. Furthermore, in gapped Dirac materials (for example, graphene nanoribbon arrays), the interplay between Berry curvature and electron–electron interactions yields nonreciprocal edge chiral Berry plasmons without the need for an external magnetic field[94,95]. Chiral Berry plasmons with chirality are manifested in split energy dispersions for oppositely directed plasmon waves. These topological and nonreciprocal phenomena are being experimentally explored for a new generation of on-chip robust nanophotonic waveguides and integrated nonreciprocal nanophotonic devices.

## Electron-driven polariton sources

Fast electrons with speeds larger than the phase velocity of the electromagnetic wave supported in the medium may result in Cherenkov radiation (CR), which has important applications in particle detection and as a radiation source. Recently, the on-chip polaritonic CR effect has been predicted in vdW materials, such as electric tunable CR-SPPs on graphene[96,97] and backward (inverse) CR-PhPs in the first reststrahlen band of hBN[98], as well as rotational, tunable and threshold-free CR-PhPs in α-$MoO_3$ (Fig. 5c). Owing to the ultra-slow velocity of vdW polaritons, only a low-energy (small velocity) electron beam is required, and the CR polaritons exhibit enhanced electro-optical conversion efficiency and even dynamic tunability. Furthermore, conventionally forbidden transitions at the atomic scale can occur over very short timescales within two-dimensional systems that support plasmons[99,100]. Recently, tunable free-electron X-ray radiation from vdW materials has been demonstrated using both theory and experiments[101]. These studies foresee opportunities to develop on-chip electron-driven sources for the mid-infrared to the X-ray region[102]. In addition, we predict that some other types of radiation[103–105] (for example, diffraction radiation, Smith–Purcell radiation and transition radiation) can also be generated by the appropriate generation of vdW photonic crystals and metasurfaces.

## Optical sensing

The high sensitivity of ultra-confined polaritons on a dielectric background and subwavelength polariton resonators could enable their use as a platform for strong light–matter interaction for sensing and surface-enhanced infrared absorption spectroscopy[4–6]. vdW polaritons are mostly located in the infrared region, in which the fingerprints of many biomolecules are found. Specifically, graphene plasmon resonance has enabled the label-free and ultrasensitive detection of proteins[4] (Fig. 5d) and inorganic molecules[106] and the identification of gases[107]. One issue with graphene resonators is their low $Q$ factor ($\omega_{res}/\Delta\omega_{res}$, in which $\omega_{res}$ is the localized polariton resonance frequency), which is almost inevitable due to the intrinsic Ohmic losses from the scattering of free electrons. By contrast, phonon polaritons in polar crystals do not suffer from Ohmic loss in principle and are bounded

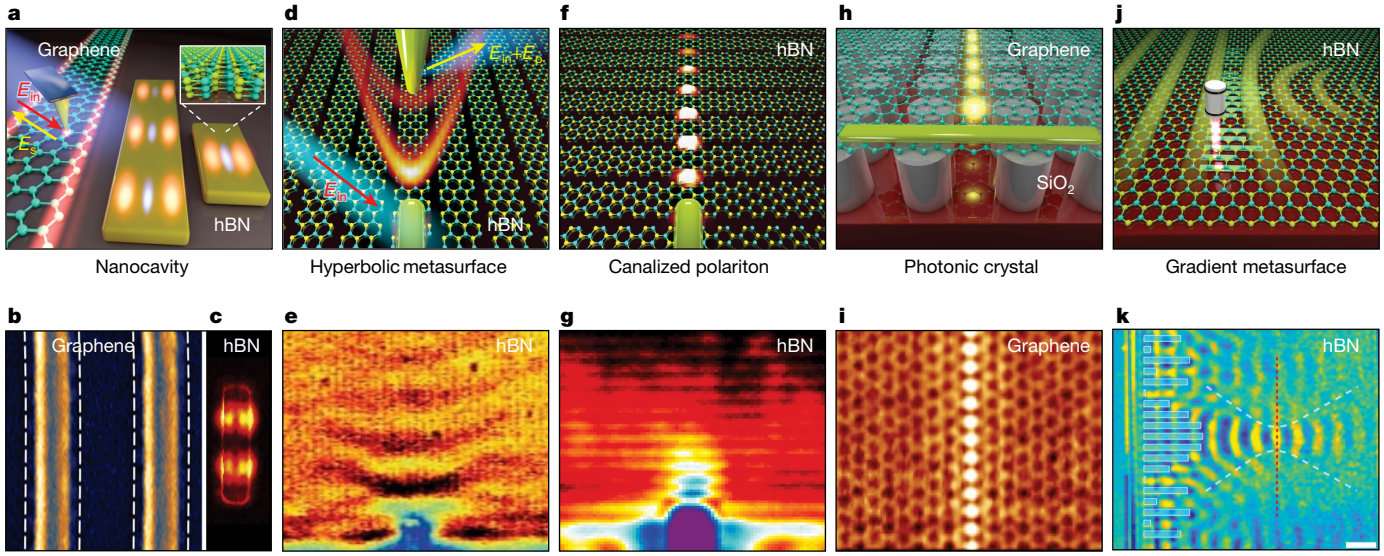


**Fig. 3 | Meta-optics based on polaritonic vdW nanostructures and heterostructures. a**–**c**, Individual vdW nanocavities (that is, graphene and hBN nanoribbon) supporting propagative and localized polariton modes. **d**, **e**, Ribbon-based vdW metasurface supporting in-plane hyperbolic polaritons. **f**, **g**, Ribbon-based vdW metasurface exhibiting strong collective polaritonic near-field coupling and thus supporting canalized polaritons. **h**, **i**, Subwavelength-scale polaritonic crystal by covering vdW materials on an array of dielectric photonic crystal. **j**, **k**, Direct laser-writing of dielectric nanostructures for vdW-polariton-based planar metalenses. **b**, Image adapted with permission from ref. [50], Hu, F. et al. *Nano Lett.* **17**, 5423–5428 (2017). Copyright 2017 American Chemical Society. **c**, Image adapted from ref. [7], Springer Nature. **e**, Image adapted from ref. [36], AAAS. **g**, Image adapted from ref. [57], Springer Nature. **i**, Image adapted from ref. [60], Springer Nature. **k**, Image adapted from ref. [34], Springer Nature.

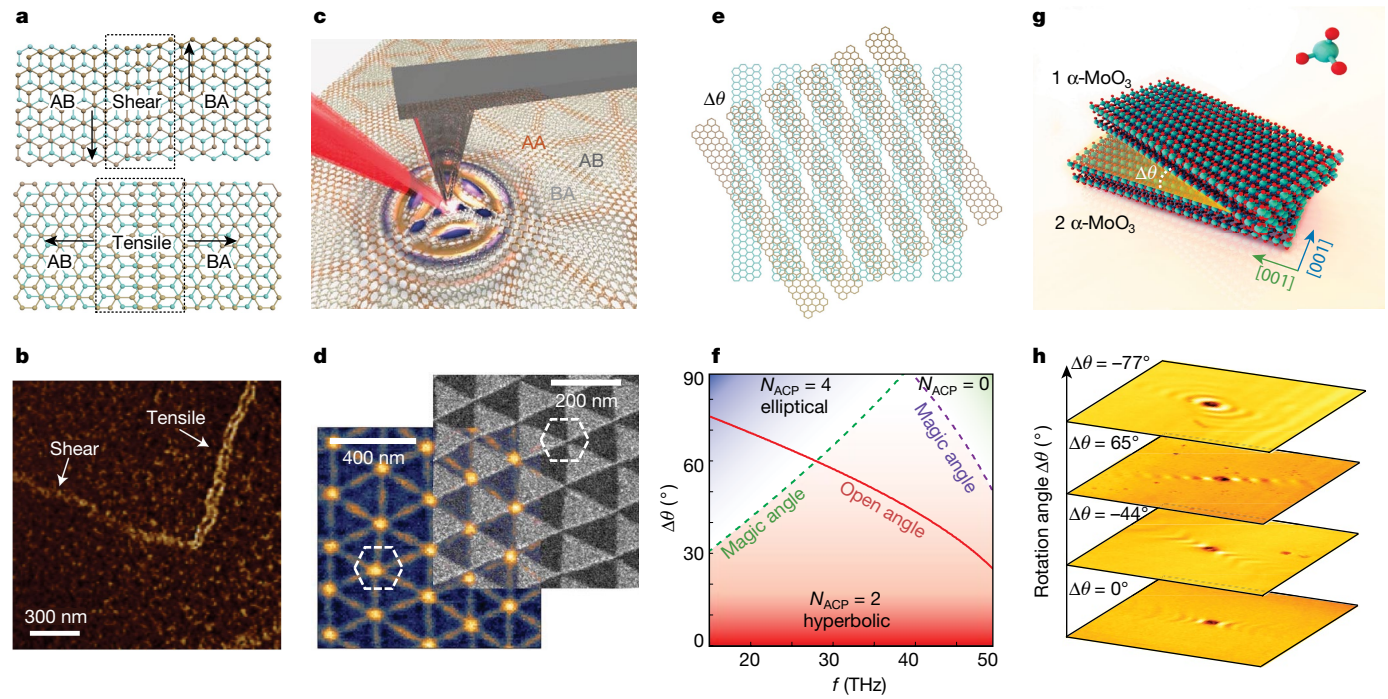


**Fig. 4 | Interlayer effects and moiré engineering for extreme polariton dispersion. a**, Shear (top) and tensile (bottom) domain-wall solitons, separating AB and BA stacking. The dislocation is parallel to the domain wall in shear strain but perpendicular to tensile strain. **b**, A sharply bent L-shape domain wall. One segment shows single-bright-line features (shear), whereas the other segment rotated by 90° shows double-bright-line features (tensile). **c**, Schematic of near-field nano-imaging of nanolight photonic crystal formed by a network of solitons in TBG. **d**, Real-space image of the nanolight photonic crystal in TBG. The contrast is due to enhanced local optical conductivity at solitons. Overlaid is the dark-field transmission electron microscopy image of a TBG sample. The dashed hexagon denotes the unit cell. **e**, Twisted bilayer hyperbolic metasurfaces. Each metasurface is composed of densely packed graphene nanoribbon arrays. **f**, Theoretical dispersion of plasmon polaritons in twisted bilayer metasurfaces plotted with the rotation angle. **g**, Twisted bilayered α-$MoO_3$. **h**, Real-space images of phonon polaritons at 903.8 $cm^{-1}$. The polariton propagation is hyperbolic at rotation angles of 0° and 44° but elliptical at 77°. At 65°, polariton canalization emerges due to the flattened dispersion. **b**, Image adapted from ref. [72], Springer Nature. **c**, **d**, Image adapted from ref. [33], AAAS. **e**, **f**, Image adapted with permission from ref. [84], Hu, G. et al., *Nano Lett.* **20**, 3217–3224 (2020). Copyright 2020 American Chemical Society. **g**, **h**, Image adapted from ref. [56], Springer Nature.

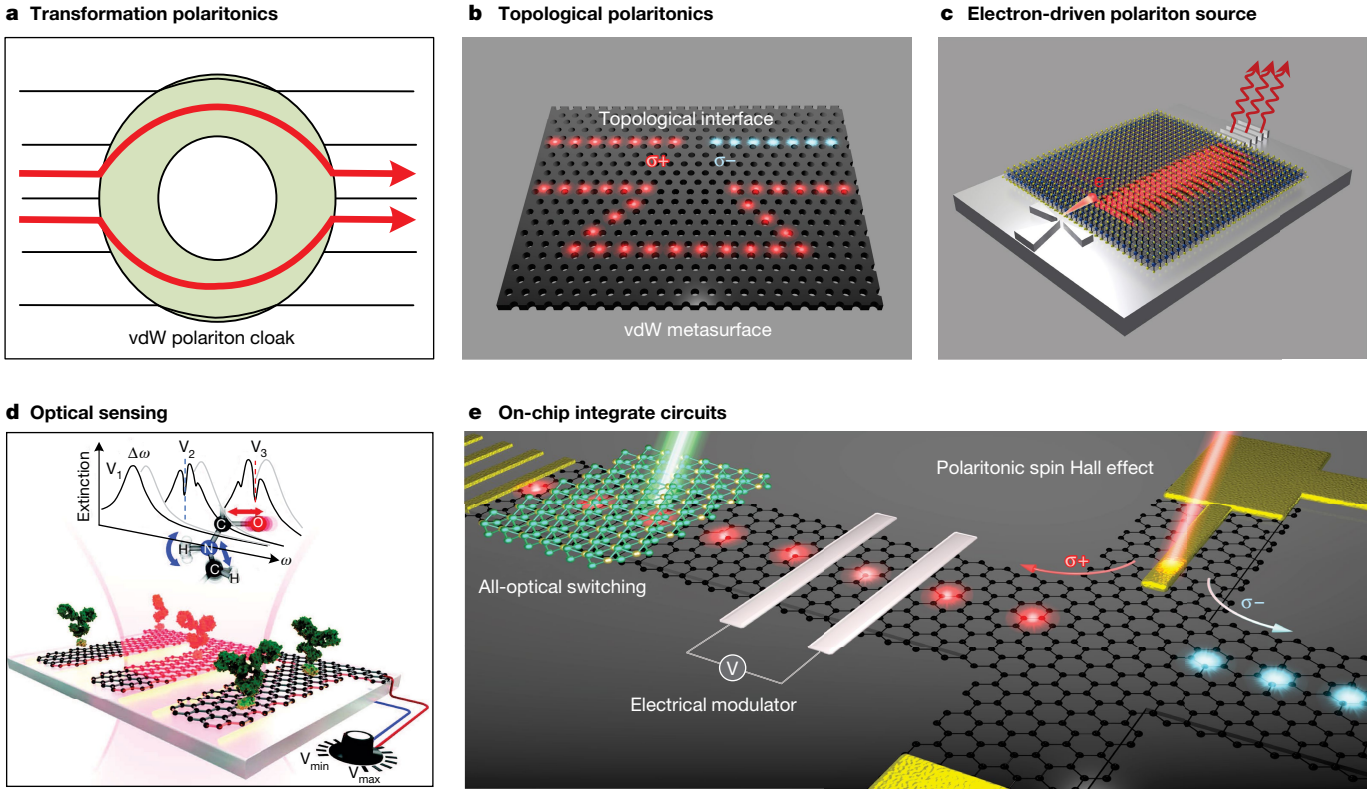


**Fig. 5 | Potential applications and future developments. a**, Planar meta-optics enables spatial dispersion engineering for transformation polaritons. **b**, Topologically protected unidirectional polariton transport at the domain-wall interface in nanostructured vdW metasurfaces, σ+ (and σ−) are left (and right) hand circularly polarized light. **c**, Unidirectional and low-threshold Cherenkov polariton radiation in α-$MoO_3$ may behave as an electron-driven polariton source for the mid-infrared region. **d**, Localized plasmon resonance in graphene nanoribbons inspired electric tunable infrared biosensors. **e**, All-optical polariton switching, electrical optical modulators and polaritonic spin Hall effect devices for on-chip integrated optical circuits. **d**, Image adapted from ref. [4], AAAS.

only by the phonon–phonon scattering loss channel. Therefore, high *Q* factors of up to 200 can be obtained in hBN and α-$MoO_3$ polaritonic cavities[41,108], which could easily reach the strong coupling regime to high-sensitivity sensing[6]. Nevertheless, an exciting regime has not been explored yet when such vdW material cavities are combined with metallic surfaces to support acoustic plasmon[25,26,39,109,110] or phonon[111] resonances. Acoustic plasmons and phonons have an extreme level of field confinement and substantially enhance the vibrational fingerprints of sub-nanometre-thick molecule layers, which can harness the ultimate level of light–matter interactions for sensing and infrared spectroscopy. Furthermore, on-chip sensing with propagating modes has been theoretically proposed to support broadband sensing capabilities[112], which only recently have been supported by initial proof-of-concept experiments[113]. Moreover, chiral plasmons have been predicted in TBGs with estimated near-field chirality several orders of magnitude larger than that of far-field circular polarized light[114,115]. This enhanced near-field chirality may promote the interaction and detection of chiral molecules, and such an approach can be extended to other twisted vdW heterostructures beyond TBGs, providing new platforms for optical sensing, chiral chemistry and beyond.

## Polaritonic spin Hall effect

Current experimental studies based on vdW polaritons use linear polarized or unpolarized infrared light. Switchable and unidirectional vdW polariton devices can be designed using spin-momentum locking with circularly polarized sources, known as the polaritonic spin Hall effect[116]. The polaritonic spin Hall effect has been experimentally achieved for metal plasmons[117], and has been recently predicted in both isotropic and anisotropic vdW polariton waves[84,118], which may lead to intriguing phenomena and applications in unidirectional waveguiding, metrology and quantum technologies. As a conceptual example (Fig. 5e, right), we can use a circularly polarized laser source to obliquely illuminate a single slit to mimic a circular dipole source. As a result, the unidirectional launching of vdW polaritons can be realized, and the propagating direction is switchable with the circular polarization of the light. This renders the polarization a new degree of freedom (a potential logical gate) to control the flow of polariton waves.

## On-chip integrated circuits

Extreme vdW polaritons have shown ubiquitous advantages in all-optical switching[11,119,120] and electro-optical modulators[10,12–14] (Fig. 5e). In particular, electrically tunable polariton devices represent an opportunity for both the semiconductor manufacturing and optical nanocircuit industries, which could potentially work together on disruptive innovations. From an integration perspective, it will be of interest to see how compact footprint and complex functionalities can ultimately be achieved over a single chip by integrating vdW materials and complementary metal–oxide–semiconductor technology. In addition, controlling, detecting and generating propagating polaritons by all-electrical means is at the heart of on-chip nano-optical processing. Electrical generation of optical plasmon modes has been predicted in double-layer graphene[121]. Direct reading of polariton modes through photocurrent signals is possible[37,3839]. More importantly, voltage-tunable phased arrays on graphene enable the in situ control of plasmons[46], which offers possibilities for ultracompact programmable polariton devices as optical counterparts to field-programmable gate arrays. We anticipate that the artificial structuring and patterning, possibly in combination with the polariton spin Hall effect and valley

Hall effect of transition metal dichalcogenide excitons, will generate previously unrealized optical nanocircuit functionalities, potentially on-chip.

However, considerable challenges remain to be addressed before vdW polariton devices can be translated from laboratory research into commercial success. One practical challenge is the propagation loss (damping) of polariton waves, which limits both the footprint and device efficiency. With increasing interest in two-dimensional materials, low-loss polaritons continue to be discovered. Today they can propagate over dozens of polariton wavelengths[88,122,123], which supports the realization of some compact and practical on-chip photonic circuits and device functionalities. Another challenge is that almost all of the devices that we discuss here are based on manual mechanical exfoliation and transfer techniques. Future technologies must enable scalability, for instance through the growth and/or deposition of large-area and high-quality vdW layers, or through the recently discovered ghost hyperbolic polaritons in conventional bulk anisotropic crystals[124].


1. Basov, D. N., Fogler, M. M. & García de Abajo, F. J. Polaritons in van der Waals materials. *Science* **354**, aag1992 (2016).
2. Low, T. et al. Polaritons in layered two-dimensional materials. *Nat. Mater.* **16**, 182–194 (2017).
**Refs.[1,2] are two comprehensive reviews of early-stage research on polaritons in natural vdW materials—including monolayers, thin slabs and hybrid heterostructures—summarizing the unique physical features of different types of vdW polariton**.
3. Dai, Z. et al. Artificial metaphotonics born naturally in two dimensions. *Chem. Rev.* **120**, 6197–6246 (2020).
4. Rodrigo, D. et al. Mid-infrared plasmonic biosensing with graphene. *Science* **349**, 165–168 (2015).
5. Hu, H. et al. Far-field nanoscale infrared spectroscopy of vibrational fingerprints of molecules with graphene plasmons. *Nat. Commun.* **7**, 12334 (2016).
6. Autore, M. et al. Boron nitride nanoresonators for phonon-enhanced molecular vibrational spectroscopy at the strong coupling limit. *Light Sci. Appl.* **7**, 17172 (2018).
7. Alfaro-Mozaz, F. J. et al. Nanoimaging of resonating hyperbolic polaritons in linear boron nitride antennas. *Nat. Commun.* **8**, 15624 (2017).
8. Li, P. et al. Hyperbolic phonon-polaritons in boron nitride for near-field optical imaging and focusing. *Nat. Commun.* **6**, 7507 (2015).
9. Dai, S. et al. Subdiffractional focusing and guiding of polaritonic rays in a natural hyperbolic material. *Nat. Commun.* **6**, 6963 (2015).
10. Liu, M. et al. A graphene-based broadband optical modulator. *Nature* **474**, 64–67 (2011).
11. Ni, G. et al. Ultrafast optical switching of infrared plasmon polaritons in high-mobility graphene. *Nat. Photonics* **10**, 244–247 (2016).
12. Yao, B. et al. Broadband gate-tunable terahertz plasmons in graphene heterostructures. *Nat. Photonics* **12**, 22–28 (2018).
13. Phare, C. T., Lee, Y.-H. D., Cardenas, J. & Lipson, M. Graphene electro-optic modulator with 30 GHz bandwidth. *Nat. Photonics* **9**, 511–514 (2015).
14. Ansell, D. et al. Hybrid graphene plasmonic waveguide modulators. *Nat. Commun.* **6**, 8846 (2015).
15. Wu, S. et al. Monolayer semiconductor nanocavity lasers with ultralow thresholds. *Nature* **520**, 69–72 (2015).
16. Chakraborty, S. et al. Gain modulation by graphene plasmons in aperiodic lattice lasers. *Science* **351**, 246–248 (2016).
17. Kurman, Y. et al. Control of semiconductor emitter frequency by increasing polariton momenta. *Nat. Photonics* **12**, 423–429 (2018).
18. Brar, V. W. et al. Hybrid surface-phonon-plasmon polariton modes in graphene/monolayer h-BN heterostructures. *Nano Lett.* **14**, 3876–3880 (2014).
19. Dai, S. et al. Graphene on hexagonal boron nitride as a tunable hyperbolic metamaterial. *Nat. Nanotechnol.* **10**, 682–686 (2015).
20. Woessner, A. et al. Highly confined low-loss plasmons in graphene–boron nitride heterostructures. *Nat. Mater.* **14**, 421–425 (2015).
21. Dubrovkin, A. M., Qiang, B., Krishnamoorthy, H. N. S., Zheludev, N. I. & Wang, Q. J. Ultra-confined surface phonon polaritons in molecular layers of van der Waals dielectrics. *Nat. Commun.* **9**, 1762 (2018).
22. Chaudhary, K. et al. Engineering phonon polaritons in van der Waals heterostructures to enhance in-plane optical anisotropy. *Sci. Adv.* **5**, eaau7171 (2019).
23. Caldwell, J. D. et al. Atomic-scale photonic hybrids for mid-infrared and terahertz nanophotonics. *Nat. Nanotechnol.* **11**, 9–15 (2016).
24. Yan, H. et al. Damping pathways of mid-infrared plasmons in graphene nanostructures. *Nat. Photonics* **7**, 394–399 (2013).
25. Alcaraz Iranzo, D. et al. Probing the ultimate plasmon confinement limits with a van der Waals heterostructure. *Science* **360**, 291–295 (2018).
26. Epstein, I. et al. Far-field excitation of single graphene plasmon cavities with ultracompressed mode volumes. *Science* **368**, 1219–1223 (2020).
27. Chen, J. et al. Optical nano-imaging of gate-tunable graphene plasmons. *Nature* **487**, 77–81 (2012).
28. Fei, Z. et al. Gate-tuning of graphene plasmons revealed by infrared nano-imaging. *Nature* **487**, 82–85 (2012).
**Refs.[27,28] independently demonstrated real-space imaging of surface plasmon polaritons in graphene**.
29. Alonso-González, P. et al. Controlling graphene plasmons with resonant metal antennas and spatial conductivity patterns. *Science* **344**, 1369–1373 (2014).
30. Yoxall, E. et al. Direct observation of ultraslow hyperbolic polariton propagation with negative phase velocity. *Nat. Photonics* **9**, 674 (2015).
31. Nikitin, A. et al. Real-space mapping of tailored sheet and edge plasmons in graphene nanoresonators. *Nat. Photonics* **10**, 239–243 (2016).
32. Ni, G. X. et al. Plasmons in graphene moiré superlattices. *Nat. Mater.* **14**, 1217–1222 (2015).
33. Sunku, S. S. et al. Photonic crystals for nano-light in moiré graphene superlattices. *Science* **362**, 1153–1156 (2018).
34. Chaudhary, K. et al. Polariton nanophotonics using phase-change materials. *Nat. Commun.* **10**, 4487 (2019).
35. Zheng, Z. et al. A mid-infrared biaxial hyperbolic van der Waals crystal. *Sci. Adv.* **5**, eaav8690 (2019).
36. Li, P. et al. Infrared hyperbolic metasurface based on nanostructured van der Waals materials. *Science* **359**, 892–896 (2018).
37. Lundeberg, M. B. et al. Thermoelectric detection and imaging of propagating graphene plasmons. *Nat. Mater.* **16**, 204–207 (2017).
38. Woessner, A. et al. Electrical detection of hyperbolic phonon-polaritons in heterostructures of graphene and boron nitride. *npj 2D Mater. Appl.* **1**, 25 (2017).
39. Alonso-González, P. et al. Acoustic terahertz graphene plasmons revealed by photocurrent nanoscopy. *Nat. Nanotechnol.* **12**, 31–35 (2017).
40. Ambrosio, A. et al. Mechanical detection and imaging of hyperbolic phonon polaritons in hexagonal boron nitride. *ACS Nano* **11**, 8741–8746 (2017).
41. Tamagnone, M. et al. Ultra-confined mid-infrared resonant phonon polaritons in van der Waals nanostructures. *Sci. Adv.* **4**, eaat7189 (2018).
42. Govyadinov, A. A. et al. Probing low-energy hyperbolic polaritons in van der Waals crystals with an electron microscope. *Nat. Commun.* **8**, 95 (2017).
43. Li, N. et al. Direct observation of highly confined phonon polaritons in suspended monolayer hexagonal boron nitride. *Nat. Mater.* **20**, 43–48 (2021).
44. Dong, W. et al. Broad-spectral-range sustainability and controllable excitation of hyperbolic phonon polaritons in α-$MoO_3$. *Adv. Mater.* **32**, 2002014 (2020).
45. Folland, T. G. et al. Reconfigurable infrared hyperbolic metasurfaces using phase change materials. *Nat. Commun.* **9**, 4371 (2018).
46. Woessner, A. et al. Electrical 2π phase control of infrared light in a 350-nm footprint using graphene plasmons. *Nat. Photonics* **11**, 421–424 (2017).
47. Vakil, A. & Engheta, N. Transformation optics using graphene. *Science* **332**, 1291–1294 (2011).
48. Lin, X. et al. All-angle negative refraction of highly squeezed plasmon and phonon polaritons in graphene-boron nitride heterostructures. *Proc. Natl Acad. Sci. USA* **114**, 6717–6721 (2017).
49. Zhang, Q. et al. Negative refraction inspired polariton lens in van der Waals lateral heterojunctions. *Appl. Phys. Lett.* **114**, 221101 (2019).
50. Hu, F. et al. Imaging the localized plasmon resonance modes in graphene nanoribbons. *Nano Lett.* **17**, 5423–5428 (2017).
51. Dai, Z. et al. Edge-oriented and steerable hyperbolic polaritons in anisotropic van der Waals nanocavities. *Nat. Commun.* **11**, 6086 (2020).
52. Dolado, I. et al. Nanoscale guiding of infrared light with hyperbolic volume and surface polaritons in van der Waals material ribbons. *Adv. Mater.* **32**, 1906530 (2020).
53. Kloppstech, K. et al. Giant heat transfer in the crossover regime between conduction and radiation. *Nat. Commun.* **8**, 14475 (2017).
54. Dias, E. J. C., Yu, R. & García de Abajo, F. J. Thermal manipulation of plasmons in atomically thin films. *Light Sci. Appl.* **9**, 87 (2020).
55. Gomez-Diaz, J. S., Tymchenko, M. & Alù, A. Hyperbolic plasmons and topological transitions over uniaxial metasurfaces. *Phys. Rev. Lett.* **114**, 233901 (2015).
56. Hu, G. et al. Topological polaritons and photonic magic angles in twisted α-$MoO_3$ bilayers. *Nature* **582**, 209–213 (2020).
57. Li, P. et al. Collective near-field coupling and nonlocal phenomena in infrared-phononic metasurfaces for nano-light canalization. *Nat. Commun.* **11**, 3663 (2020).
58. Cortes, C. L. & Jacob, Z. Super-Coulombic atom–atom interactions in hyperbolic media. *Nat. Commun.* **8**, 14144 (2017).
59. Alfaro-Mozaz, F. J. et al. Deeply subwavelength phonon-polaritonic crystal made of a van der Waals material. *Nat. Commun.* **10**, 42 (2019).
60. Xiong, L. et al. Photonic crystal for graphene plasmons. *Nat. Commun.* **10**, 4780 (2019).
61. Li, P. et al. Reversible optical switching of highly confined phonon-polaritons with an ultrathin phase-change material. *Nat. Mater.* **15**, 870–875 (2016).
62. Cao, Y. et al. Unconventional superconductivity in magic-angle graphene superlattices. *Nature* **556**, 43–50 (2018).
63. Cao, Y. et al. Correlated insulator behaviour at half-filling in magic-angle graphene superlattices. *Nature* **556**, 80–84 (2018).
64. Tran, K. et al. Evidence for moiré excitons in van der Waals heterostructures. *Nature* **567**, 71–75 (2019).
65. Seyler, K. L. et al. Signatures of moiré-trapped valley excitons in $MoSe_2$/$WSe_2$ heterobilayers. *Nature* **567**, 66–70 (2019).
66. Jin, C. et al. Observation of moiré excitons in $WSe_2$/$WS_2$ heterostructure superlattices. *Nature* **567**, 76–80 (2019).
67. Alexeev, E. M. et al. Resonantly hybridized excitons in moiré superlattices in van der Waals heterostructures. *Nature* **567**, 81–86 (2019).
68. Aoki, M. & Amawashi, H. Dependence of band structures on stacking and field in layered graphene. *Solid State Commun.* **142**, 123–127 (2007).
69. Zhang, F., Jung, J., Fiete, G. A., Niu, Q. & MacDonald, A. H. Spontaneous quantum Hall states in chirally stacked few-layer graphene systems. *Phys. Rev. Lett.* **106**, 156801 (2011).
70. Ju, L. et al. Topological valley transport at bilayer graphene domain walls. *Nature* **520**, 650–655 (2015).
71. Jiang, L. et al. Manipulation of domain-wall solitons in bi- and trilayer graphene. *Nat. Nanotechnol.* **13**, 204–208 (2018).
72. Jiang, L. et al. Soliton-dependent plasmon reflection at bilayer graphene domain walls. *Nat. Mater.* **15**, 840–844 (2016).
73. Hu, F. et al. Real-space imaging of the tailored plasmons in twisted bilayer graphene. *Phys. Rev. Lett.* **119**, 247402 (2017).

74. Ni, G. X. et al. Soliton superlattices in twisted hexagonal boron nitride. *Nat. Commun.* **10**, 4360 (2019).
75. Luo, Y. et al. In situ nanoscale imaging of moiré superlattices in twisted van der Waals heterostructures. *Nat. Commun.* **11**, 4209 (2020).
76. Chen, X. et al. Moiré engineering of electronic phenomena in correlated oxides. *Nat. Phys.* **16**, 631–635 (2020).
77. Sunku, S. S. et al. Nano-photocurrent mapping of local electronic structure in twisted bilayer graphene. *Nano Lett.* **20**, 2958–2964 (2020).
78. McGilly, L. J. et al. Visualization of moiré superlattices. *Nat. Nanotechnol.* **15**, 580–584 (2020).
79. Lewandowski, C. & Levitov, L. Intrinsically undamped plasmon modes in narrow electron bands. *Proc. Natl Acad. Sci. USA* **116**, 20869–20874 (2019).
80. Khaliji, K., Stauber, T. & Low, T. Plasmons and screening in finite-bandwidth two-dimensional electron gas. *Phys. Rev. B* **102**, 125408 (2020).
81. Brey, L., Stauber, T., Slipchenko, T. & Martín-Moreno, L. Plasmonic Dirac cone in twisted bilayer graphene. *Phys. Rev. Lett.* **125**, 256804 (2020).
82. Woods, C. et al. Commensurate–incommensurate transition in graphene on hexagonal boron nitride. *Nat. Phys.* **10**, 451–456 (2014).
83. Kennes, D. M. et al. Moiré heterostructures as a condensed-matter quantum simulator. *Nat. Phys.* **17**, 155–163 (2021).
84. Hu, G., Krasnok, A., Mazor, Y., Qiu, C.-W. & Alù, A. Moiré hyperbolic metasurfaces. *Nano Lett.* **20**, 3217–3224 (2020).
85. Kotov, O. & Lozovik, Y. E. Hyperbolic hybrid waves and optical topological transitions in few-layer anisotropic metasurfaces. *Phys. Rev. B* **100**, 165424 (2019).
86. Zheng, Z. et al. Phonon polaritons in twisted double-layers of hyperbolic van der Waals crystals. *Nano Lett.* **20**, 5301–5308 (2020).
87. Duan, J. et al. Twisted nano-optics: manipulating light at the nanoscale with twisted phonon polaritonic slabs. *Nano Lett.* **20**, 5323–5329 (2020).
88. Ma, W. et al. In-plane anisotropic and ultra-low-loss polaritons in a natural van der Waals crystal. *Nature* **562**, 557–562 (2018).
89. Pendry, J. B., Schurig, D. & Smith, D. R. Controlling electromagnetic fields. *Science* **312**, 1780–1782 (2006).
90. Schurig, D. et al. Metamaterial electromagnetic cloak at microwave frequencies. *Science* **314**, 977–980 (2006).
91. Alù, A. & Engheta, N. Achieving transparency with plasmonic and metamaterial coatings. *Phys. Rev. E* **72**, 016623 (2005).
92. Jin, D. et al. Infrared topological plasmons in graphene. *Phys. Rev. Lett.* **118**, 245301 (2017).
93. Liu, W. et al. Generation of helical topological exciton-polaritons. *Science* **370**, 600–604 (2020).
94. Kumar, A. et al. Chiral plasmon in gapped Dirac systems. *Phys. Rev. B* **93**, 041413 (2016).
95. Song, J. C. & Rudner, M. S. Chiral plasmons without magnetic field. *Proc. Natl Acad. Sci. USA* **113**, 4658–4663 (2016).
96. Kaminer, I. et al. Efficient plasmonic emission by the quantum Čerenkov effect from hot carriers in graphene. *Nat. Commun.* **7**, ncomms11880 (2016).
97. Tao, J., Wu, L. & Zheng, G. Graphene surface-polariton in-plane Cherenkov radiation. *Carbon* **133**, 249–253 (2018).
98. Tao, J., Wu, L., Zheng, G. & Yu, S. Cherenkov polaritonic radiation in a natural hyperbolic material. *Carbon* **150**, 136–141 (2019).
99. Rivera, N., Kaminer, I., Zhen, B., Joannopoulos, J. D. & Soljačić, M. Shrinking light to allow forbidden transitions on the atomic scale. *Science* **353**, 263–269 (2016).
100. Lin, X. et al. Splashing transients of 2D plasmons launched by swift electrons. *Sci. Adv.* **3**, e1601192 (2017).
101. Shentcis, M. et al. Tunable free-electron X-ray radiation from van der Waals materials. *Nat. Photonics* **14**, 686–692 (2020).
102. Wong, L. J., Kaminer, I., Ilic, O., Joannopoulos, J. D. & Soljačić, M. Towards graphene plasmon-based free-electron infrared to X-ray sources. *Nat. Photonics* **10**, 46–52 (2016).
103. Rosolen, G. et al. Metasurface-based multi-harmonic free-electron light source. *Light Sci. Appl.* **7**, 64 (2018).
104. Li, Y., Ferreyra, P., Swan, A. K. & Paiella, R. Current-driven terahertz light emission from graphene plasmonic oscillations. *ACS Photonics* **6**, 2562–2569 (2019).
105. Yang, Y. et al. Maximal spontaneous photon emission and energy loss from free electrons. *Nat. Phys.* **14**, 894–899 (2018).
106. Farmer, D. B., Avouris, P., Li, Y., Heinz, T. F. & Han, S.-J. Ultrasensitive plasmonic detection of molecules with graphene. *ACS Photonics* **3**, 553–557 (2016).
107. Hu, H. et al. Gas identification with graphene plasmons. *Nat. Commun.* **10**, 1131 (2019).
108. Tamagnone, M. et al. High quality factor polariton resonators using van der Waals materials. Preprint at https://arxiv.org/abs/1905.02177 (2019).
109. Lee, I.-H., Yoo, D., Avouris, P., Low, T. & Oh, S.-H. Graphene acoustic plasmon resonator for ultrasensitive infrared spectroscopy. *Nat. Nanotechnol.* **14**, 313–319 (2019).
110. Lee, I.-H. et al. Anisotropic acoustic plasmons in black phosphorus. *ACS Photonics* **5**, 2208–2216 (2018).
111. Yuan, Z. et al. Extremely-confined acoustic phonon polaritons in monolayer-hBN/metal heterostructures for strong light-matter interactions. *ACS Photonics* **7**, 2610–2617 (2020).
112. Francescato, Y., Giannini, V., Yang, J., Huang, M. & Maier, S. A. Graphene sandwiches as a platform for broadband molecular spectroscopy. *ACS Photonics* **1**, 437–443 (2014).
113. Bylinkin, A. et al. Real-space observation of vibrational strong coupling between propagating phonon polaritons and organic molecules. *Nat. Photonics* **15**, 197–202 (2021).
114. Lin, X. et al. Chiral plasmons with twisted atomic bilayers. *Phys. Rev. Lett.* **125**, 077401 (2020).
115. Stauber, T., Low, T. & Gómez-Santos, G. Plasmon-enhanced near-field chirality in twisted van der Waals heterostructures. *Nano Lett.* **20**, 8711–8718 (2020).
116. Lin, J. et al. Polarization-controlled tunable directional coupling of surface plasmon polaritons. *Science* **340**, 331–334 (2013).
117. Rodríguez-Fortuño, F. J. et al. Near-field interference for the unidirectional excitation of electromagnetic guided modes. *Science* **340**, 328–330 (2013).
118. Nemilentsau, A., Stauber, T., Gómez-Santos, G., Luskin, M. & Low, T. Switchable and unidirectional plasmonic beacons in hyperbolic two-dimensional materials. *Phys. Rev. B* **99**, 201405 (2019).
119. Huber, M. A. et al. Femtosecond photo-switching of interface polaritons in black phosphorus heterostructures. *Nat. Nanotechnol.* **12**, 207–211 (2017).
120. Klein, M. et al. 2D semiconductor nonlinear plasmonic modulators. *Nat. Commun.* **10**, 3264 (2019).
121. Guerrero-Becerra, K. A., Tomadin, A. & Polini, M. Electrical plasmon injection in double-layer graphene heterostructures. *Phys. Rev. B* **100**, 125434 (2019).
122. Ni, G. X. et al. Fundamental limits to graphene plasmonics. *Nature* **557**, 530–533 (2018).
123. Giles, A. J. et al. Ultralow-loss polaritons in isotopically pure boron nitride. *Nat. Mater.* **17**, 134–139 (2018).
124. Weiliang, M. G. et al. Ghost hyperbolic surface polaritons in bulk anisotropic crystals. *Nature* **596**, 362-366 (2021).
**This reference reports the first observation of ghost polaritons and the first real-space mapping of the hyperbolic plaritons in bulk anisotropic crystals, which demonstrates approximately 20-μm long-range propagation at room temperature and large-scale production readiness for polaritonic on-chip devices.**
125. Dai, S. et al. Tunable phonon polaritons in atomically thin van der Waals crystals of boron nitride. *Science* **343**, 1125–1129 (2014).
126. Hu, F. et al. Imaging exciton–polariton transport in $MoSe_2$ waveguides. *Nat. Photonics* **11**, 356–360 (2017).
127. Low, T. et al. Plasmons and screening in monolayer and multilayer black phosphorus. *Phys. Rev. Lett.* **113**, 106802 (2014).
128. Nemilentsau, A., Low, T. & Hanson, G. Anisotropic 2D materials for tunable hyperbolic plasmonics. *Phys. Rev. Lett.* **116**, 066804 (2016).
129. Wang, C. et al. Van der Waals thin films of $WTe_2$ for natural hyperbolic plasmonic surfaces. *Nat. Commun.* **11**, 1158 (2020).
130. Zheng, Z. et al. Highly confined and tunable hyperbolic phonon polaritons in van der Waals semiconducting transition metal oxides. *Adv. Mater.* **30**, 1705318 (2018).
131. Álvarez-Pérez, G. et al. Infrared permittivity of the biaxial van der Waals semiconductor α-$MoO_3$ from near- and far-field correlative studies. *Adv. Mater.* **32**, 1908176 (2020).
132. Taboada-Gutiérrez, J. et al. Broad spectral tuning of ultra-low-loss polaritons in a van der Waals crystal by intercalation. *Nat. Mater.* **19**, 964–968 (2020).
133. Álvarez-Pérez, G., Voronin, K. V., Volkov, V. S., Alonso-González, P. & Nikitin, A. Y. Analytical approximations for the dispersion of electromagnetic modes in slabs of biaxial crystals. *Phys. Rev. B* **100**, 235408 (2019).
134. Sun, F. et al. Polariton waveguide modes in two-dimensional van der Waals crystals: an analytical model and correlative nano-imaging. *Nanoscale* **13**, 4845–4854 (2021).



**Acknowledgements** This project was supported by the National Research Foundation, Prime Minister's Office, Singapore under Competitive Research Program Award NRF-CRP22-2019-0006; the Vannevar Bush Faculty Fellowship program; the Simons Foundation; and the Air Force Office of Scientific Research MURI program. R.H. acknowledges financial support from the Spanish Ministry of Science, Innovation and Universities (national project RTI2018-094830-B-100 and the project MDM-2016-0618 of the Marie de Maeztu Units of Excellence Program) and the Basque Government (grant no. IT1164-19). P.L. acknowledges the National Natural Science Foundation of China (grant no. 62075070). G.H. acknowledges the support from A*STAR AME Young Individual Research Grants (YIRG, No. A2084c0172).


**Author contributions** Q.Z., G.H. and W.M. wrote the manuscript; P.L., A.K. and R.H. contributed to the discussion of content; and A.A. and C.-W.Q. supervised the project. All authors contributed to the editing of the paper.

**Competing interests** The authors declare no competing interests.

**Additional information**


**Correspondence and requests for materials** should be addressed to Andrea Alù or Cheng-Wei Qiu.



**Peer review information** *Nature* thanks Tony Low and the other, anonymous, reviewer(s) for their contribution to the peer review of this work.